Applied Catalysis B: Environmental 257 (2019) 117935

Contents lists available at ScienceDirect

Applied Catalysis B: Environmental

journal homepage: www.elsevier.com/locate/apcatb

Donor-acceptor type triazine-based conjugated porous polymer for visible-light-driven photocatalytic hydrogen evolution

Jie Yu[a,1], Xiaoqin Sun[a,1], Xiaoxiang Xu[a,b,*], Chi Zhang[a,*], Xiaoming He[a,*]

[a] Shanghai Key Lab of Chemical Assessment and Sustainability, School of Chemical Science and Engineering, Tongji University, 1239 Siping Road, Shanghai, 200092, China

[b] Clinical and Central Lab, Putuo People's Hospital, Tongji University, 1291 Jiangning Road, Shanghai, 200060, China

ARTICLE INFO

Keywords:
Conjugated microporous polymers
Metal-free synthesis
Photocatalyst
Water splitting
Hydrogen production

ABSTRACT

Conjugated microporous polymers (CMPs) are an emerging class of promising photocatalysts because of their large specific surface areas and adjustable optical band gaps. To avoid the metal contamination, metal-free synthetic procedure for making CMPs for photocatalytic water splitting are highly desired. Herein, we designed and synthesized two triazine-based conjugated microporous polymers P1 and P2 through a simple, efficient, metal-free catalyzed approach. Through linking donor-acceptor (D-A) type pyrazole-benzothiadiazole-pyrazole light-absorbing units by triazine units, P1 has an ideal optical band gap of about 2.3 eV and exhibits a high H_2 evolution rate (HER) of 50 μmol h^{-1} under visible light illumination ($\lambda \geq 420$ nm) and apparent quantum efficiency (AQE) as high as 3.58% at 420 ± 20 nm. In contrast, by replacing electron-neutral benzene instead of electron-withdrawing benzothiadiazole, P2 shows obvious hypochromatic shift in the absorption and large optical band gap of about 2.9 eV, as well as poor photocatalytic property.

1. Introduction

In light of the increasing global energy crisis and environmental pollution, photocatalytic water splitting has received great attention as it holds the promise to build a clean and sustainable energy infrastructure that can ultimately decarbonize our fossil-fuel based energy economics. Photocatalytic hydrogen generation from water using organic semiconductors is a rapidly growing research field [1,2]. Compared with inorganic photocatalyst [3–11], conjugated organic counterpart has distinct advantages such as low cost, nontoxicity, lightweight and facile processability. In addition, organic synthesis allows us to tune electronic and optical properties for optimization of their performance. Ever since the first linear poly(p-phenylene)s reported as a photocatalyst for hydrogen evolution in 1985 and graphitic carbon nitride (g-C_3N_4) reported on 2009 [12,13], the research of the photocatalytic water splitting using organic semiconductors were spurred. Although most of these works has focused on graphitic carbon nitride (g-C_3N_4) [14,15], other types of organic semiconductors such as linear conjugated polymers [16–20], conjugated microporous polymers (CMPs) [20–27], covalent organic frameworks (COFs) [28,29], poly (azomethine)s [30] and organic polymer dots [31,32] have been developed for efficient hydrogen production.

Recently, nitrogen-containing organic conjugated polymers have been shown to display improved photocatalytic activity in water splitting [30–40]. The incorporation of nitrogen atoms into polymeric systems has been shown to correlate with efficient hydrogen evolution, with its free electron pair and electron poor character, contributing to active reaction sites. Müllen and coworkers demonstrated three-dimensional conjugated poly(azomethine) networks for promising behaviour in photocatalytic hydrogen evolution [30]. Zwijnenburg and coworkers systematically studied how the introduction of nitrogen into poly(p-phenylene)s affected their ability to act as hydrogen evolution photocatalysts [18]. Inspired by the structure of g-C_3N_4, triazine-based conjugated polymers have drawn much attention and have been shown to generate hydrogen production with good performance during the past 5 years [33–37]. Along this side, B.V. Lotsch and co-workers have studied a series of azine-linked covalent organic frameworks with varying number of nitrogen atoms for visible light-induced hydrogen generation, suggesting the advantages of triazine-based covalent organic framework for high photocatalytic performance [38,31–40].

From a synthetic perspective, chemical reactions for synthesizing conjugated polymers heavily rely on the well-developed metal

* Corresponding authors at: Shanghai Key Lab of Chemical Assessment and Sustainability, School of Chemical Science and Engineering, Tongji University, 1239 Siping Road, Shanghai, 200092, China.

E-mail addresses: xxxu@tongji.edu.cn (X. Xu), chizhang@tongji.edu.cn (C. Zhang), xmhe@tongji.edu.cn (X. He).

[1] These authors contributed equally to this work.

https://doi.org/10.1016/j.apcatb.2019.117935
Received 13 March 2019; Received in revised form 12 June 2019; Accepted 6 July 2019
Available online 08 July 2019
0926-3373/

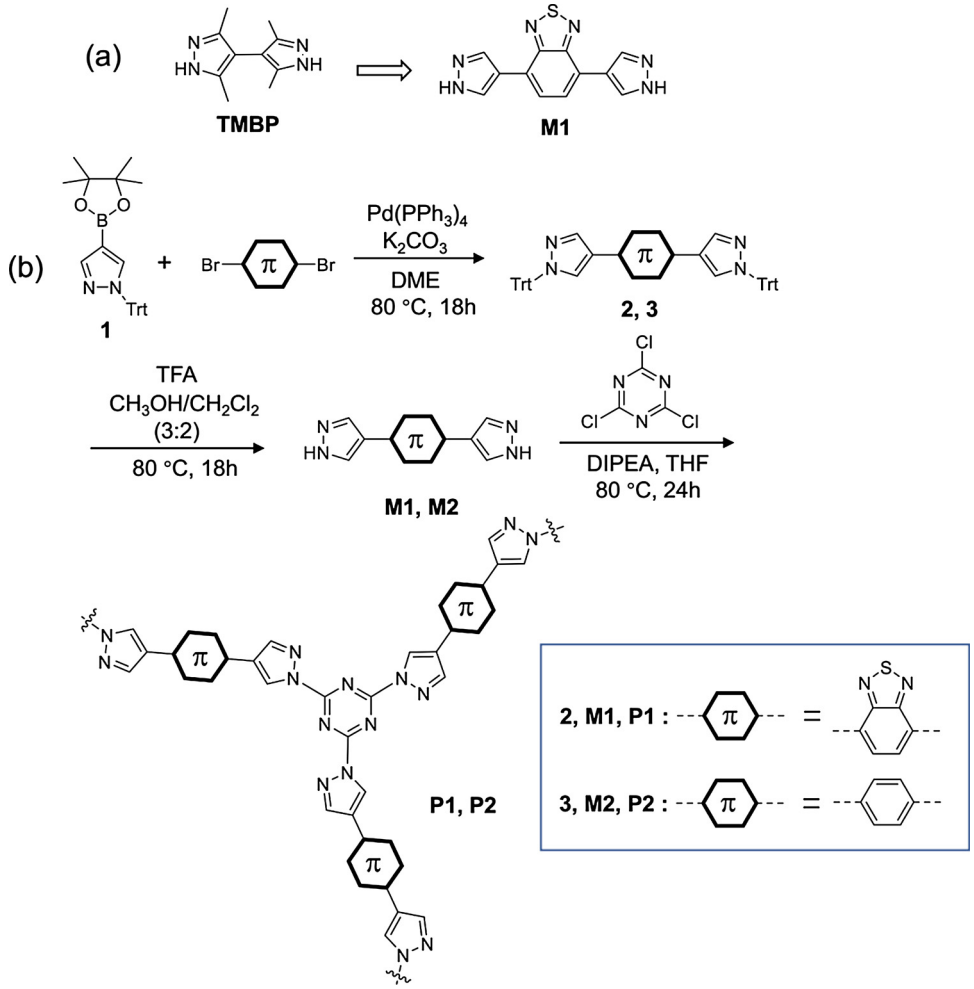

Scheme 1. (a) Structures of TMBP and M1. (b) Synthetic Scheme for P1 and P2.

catalyzed cross-coupling reactions, such as suzuki cross-coupling reaction, still cross-coupling reaction, sonogashira–hagihara reaction and Yamamoto reaction [1,41]. However, metal residues can lead to complications with electronic properties measurements or optical properties of conjugated materials, which can further influence their diverse applications. Therefore, utilization of metal-free synthetic procedure for making conjugated materials for photocatalytic water splitting are highly sought after. In this regard, while schiff-base reaction involving metal-free catalyst have been utilized to prepare organic photocatalyst [30,40]; other new metal-free synthetic approach remains considerably under-explored.

In 2014, Xu and coworkers reported an easy metal-free approach to make a porous conjugated material by reaction of cyanuric chloride and tetramethyl-4,4′-bipyrazol (TMBP, Scheme 1) in the presence of organic base [42]. Due to the presence of large torsional angle enforced by the methyl groups of TMBP, the visible-light absorption of the materials is limited. It is believed that utilization of rational designed light-absorbing monomer instead of TMBP would be able to build novel triazine-based CMP for efficient photocatalytic hydrogen generation under visible light. One common strategy to tune the optical property of conjugated materials is to design donor-acceptor (D-A) type copolymers with alternating electron-accepting units and electron-donating units along the backbone [43]. While a variety of D-A type conjugated polymers have been successfully designed and utilized for the application in organic solar cell, however they are less explored for visible-light-driven photocatalytic hydrogen evolution [43].

Herein, two porous triazine-based conjugated materials P1 and P2 (Scheme 1) have been designed and synthesized using a metal-free synthetic approach. This resultant polymer framework has unique tritopic node of the triazine and its three pyrazole neighbours, forming multiple rigid nitrogen-rich trident ligands for not only stabilizing metal cocatalyst, acting as active site for photocatalytic water splitting, but also providing hydrophilic microenvironment that allows better wettability in aqueous solution. Particularly, P1 featuring D-A type pyrazole-benzothiadiazole-pyrazole (M1, Scheme 1) light-absorbing units connected by triazine units using a metal-free synthetic approach has an ideal optical band gap of about 2.3 eV and exhibits a high H_2 evolution rate (HER) of 50 μmol h^{-1} under visible light illumination ($\lambda \geq 420$ nm) and apparent quantum efficiency (AQE) as high as 3.58% at 420 ± 20 nm. In contrast, P2 exhibits poor photocatalytic property, which is correlated to its less visible light absorption and larger optical band gap (2.9 eV) due to the absence of D-A moiety in the polymer backbone. This work enriches the metal-free synthesis of triazine-based porous polymer for photocatalytic hydrogen evolution, and highlights the importance of rational designed D-A structure on the photocatalytic performance.

2. Experimental section

2.1. Materials

All chemical reagents were purchased from commercial sources (Aldrich, Alfa Aesar, Strem Energy Chemical and Adamas) and were used as received unless otherwise noted. 4-bromo-1-trityl-1H-pyrazole [44], 1-trityl-1H-pyrazol-4-ylboronate pinacol ester [44], 1,4-bis(1H-pyrazol-4-yl)benzene (M2) [44] and 4,7-dibromobenzothiadiazole [45]

were prepared according to reported procedures. All reactions and manipulations were carried out under a dry nitrogen atmosphere employing standard Schlenk techniques.

2.2. Characterization

^{1}H NMR and ^{13}C NMR spectra were recorded on a 600 MHz BRUKER ARX600 spectrometer at room temperature, with tetramethylsilane (TMS) as the internal standard. Fourier transform infrared (FT-IR) measurement was carried out using a BRUKER ALPHA spectrophotometer with polymers dispersed in pressed KBr disks. Powder X-ray diffraction of samples was recorded using a BRUKER D2 PHASER X-ray diffractometer equipped with a Cu sealed tube (λ = 1.54184 Å) at 30 kV and 10 mA with a scan speed of 1 s/step. UV–vis absorption spectra were recorded using a SPECORD 200 PLUS (analytikjena, Germany) diode-array spectrophotometer equipped with an integrating sphere. Diffuse reflectance spectra were collected on a UV–vis spectrophotometer with integrating sphere (SHIMADZU UV-2600). Emission experiments were carried out on a HORIBA Fluorolog spectrofluorometer. Thermal gravimetric analysis (TGA) was conducted on a thermal analysis instrument (TGA Q500) under a nitrogen atmosphere at a heating rate of 10 °C min^{-1}. The morphology and size of the samples were examined by scanning electron microscopy (SEM, Hitachi S-4800). Transmission electron microscopy (TEM) measurement was conducted on a high-resolution transmission electron microscope (HRTEM, Joel-2010) operating at an acceleration voltage of 200 kV. X-ray Photoelectron Spectroscopy (XPS) was carried out on an AXIS ULTRA DLD instrument, and analyzed by the XPSPEAK41 software.

2.3. Electrochemical measurement

Cyclic voltammetry (CV) measurement was carried out on a CHI760E electrochemical workstation in a three-electrode cell system using a 0.1 M solution of tetrabutylammonium hexafluorophosphate ($TBAPF_6$) in acetonitrile as the supporting electrolyte with glassy carbon as the working electrode, Ag^+/Ag (0.01 M of $AgNO_3$ in acetonitrile) as the reference electrode and platinum wire as the counter electrode. The samples were prepared by mixing 4 mg polymer in 1 mL MeOH with 80 μL 5 wt% Nafion, the mixture was ultrasonicated and then dropped cast on a glass substrate and dried in a vacuum chamber. The CV experiment with a scan rate of 50 mV s^{-1} was conducted in the supporting electrolyte. The LUMO energy level (E_{LUMO}) was calculated from onset reduction potential according to the equation of E_{LUMO} (V vs SHE) = E (V vs $Ag/AgNO_3$ [0.01 M]) + 0.681 V [46–48].

2.4. Measurement of porous properties

Nitrogen sorption measurement and micropore analysis were carried out at 77.3 K using a Micromeritics TRISTAR 3020 adsorption analyzer. The polymers were degassed at 120 °C for 12 h under vacuum before sorption measurement. The surface area of the sample was calculated in the relative pressure (P/P_0) range of 0.05-0.20 using a Brunauer-Emmett-Teller (BET) model. The BJH desorption pore size distribution analysis method was utilized for the estimation of pore size distribution (PSD).

2.5. Measurement of photocatalytic activity

The photocatalytic hydrogen evolution test was conducted on a LabSolar-III AG reaction cell (Beijing PerfectLight Co.) using 50 mg of the prepared photocatalyst suspended in triethanolamine (TEOA) aqueous solution. Pt was applied as a co-catalyst to promote the water reduction reactions and was loaded into the sample powders by a thermal deposition method : appropriate amounts of aqueous H_2PtCl_6 solution were impregnated into the sample powders in a water bath until dryness. The temperature was then increased to 453 K for 2 h in order to convert H_2PtCl_6 into Pt. A double-walled glass reactor was equipped with a cooling water jacket to keep a constant temperature (6 °C). The suspension was irradiated using a 300 W Xe lamp (PLS-SEX300/300UV, Beijing Perfect Light Co.) coupled with AM 1.5 filter or UV-cutoff filter ($\lambda \geq$ 420 nm) for simulated sun light and visible light illumination. The yield of hydrogen was analyzed with an online gas chromatograph (GC7900, Techcomp), and Ar was used as the carrier gas.

2.6. Synthesis of 1,4-bis(1-trityl-1H-pyrazol-4-yl) benzothiadiazole (2)

To a 250 mL Schenk flask backfilled with N_2 was added 4,7-dibromobenzothiadiazole (1 g, 3.4 mmol), 1-trityl-1H-pyrazol-4-ylboronate pinacol ester (3.26 g, 7.48 mmol), K_2CO_3 (4.37 g, 31.64 mmol) and 1,2-dimethoxyethane (80 mL). The suspension was degassed for 0.5 h, before addition of $Pd(PPh_3)_4$ (90.42 mg, 0.078 mmol) and the reaction was heated to 80 °C for 18 h. After cooling down to room temperature, the solvent was removed in vacuo, the residue suspended in water and the organics were extracted into dichloromethane. The combined organic phases were dried over $MgSO_4$ and concentrated in vacuo to yield 1,4-bis(1-trityl-1H-pyrazol-4-yl) benzothiadiazole (2.1 g, 81%) as a yellow solid. ^{1}H NMR (600 MHz, $CDCl_3$): δ (ppm) = 8.43 (m, 4 H; Pz*H*), 7.70 (m, 2 H; Ar*H*), 7.40-7-20 (m, 30 H; C_6H_5). ^{13}C NMR (150 MHz, $CDCl_3$): δ (ppm) = 153.01, 146.81, 143.02, 138.26, 131.92, 130.17, 127.91, 127.89, 127.79, 124.37, 123.29, 117.46.

2.7. Synthesis of 1,4-bis(1H-pyrazol-4-yl) benzothiadiazole (M1)

To a suspension of 1,4-bis(1-trityl-1H-pyrazol-4-yl) benzothiadiazole (0.3 g, 0.4 mmol) in a mixture of methanol and dichloromethane solution (3:2 vol., 23 mL), was added trifluoroacetic acid (TFA, 6 mL, 80.78 mmol). Then the mixture was heated to reflux at 70 °C for 18 h. After cooling down to room temperature, the solvent was removed in vacuo. The resulting solid was triturated in toluene, filtered and washed with toluene, chloroform, water, methanol and finally diethyl ether (3 mL each) to yield yellow solid. Residual TFA was removed by suspending in water and the PH was adjusted to 5 with 2 M NaOH. After that, the compound was filtered and dried overnight at 50 °C to yield 1,4-bis(1H-pyrazol-4-yl) benzothiadiazole (92 mg, 84%) as a yellow powder. ^{1}H NMR (600 MHz, d6-DMSO): δ (ppm) = 8.53 (s, 4 H; Pz*H*), 8.01 (s, 2 H; Ar*H*). ^{13}C NMR (150 MHz, d6-DMSO): δ (ppm) = 152.99, 133.17, 125.28, 123.45, 117.76.

2.8. Synthesis of P1

Cyanuric chloride (110 mg, 0.6 mmol) was quickly (within 5 min) weighed in air and added to a N_2-filled 250 mL, two-neck, round bottom flask equipped with a magnetic stirring bar and a condenser. M1 (240 mg, 0.89 mmol) was then added. A mixture of N, N-diisopropylethylamine (460 mg, 3.60 mmol) and dry THF (tetrahydrofuran, 100 mL, anhydrous), previously deaerated by N_2, was then transferred into the round-bottom flask. The flask was placed in an oil-bath and the temperature of the bath was raised to 80 °C over the period of one hour. After one hour, yellow precipitate started to form. After the reaction mixture was thus stirred and refluxed (under N_2) for 23 h, the solid product was separated by suction filtration, washed with DI water (10 × 20 mL), ethanol (5 × 20 mL) and dichloromethane (5 × 20 mL), and dried in air (yellow solid, 240 mg, 80%). ^{13}C solid-state NMR (150 MHz): δ (ppm) = 160.455, 150.099, 142.869, 120.121. Elemental analysis calcd (%) for $C_{21}H_9N_{12}S_{1.5}{\cdot}5H_2O$ ($C_{21}H_9N_{12}S_{1.5}$ being one repeat unit): C 44.44, H 3.37, N 29.62; found: C 44.73, H 3.36, N 27.73.

2.9. Synthesis of P2

P2 was synthesized according to a procedure similar to that used for P1, except that M2 was used in place of M1. Subsequent wash with DI

water (10 × 20 mL), ethanol (5 × 20 mL) and dichloromethane (5 × 20 mL), gave P2 as a white solid (Yield: 65%). ^{13}C solid-state NMR (150 MHz): δ (ppm) = 141.835, 134.054, 127.933, 124.871, 122.941, 120.330. Elemental analysis calcd (%) for $C_{21}H_{12}N_9{\cdot}2H_2O$ ($C_{21}H_{15}N_6$ being one repeat unit): C 59.15, H 3.78, N 29.56; found: C 59.40, H 3.91, N 28.97.

2.10. Synthesis of 4 for model reaction

Cyanuric chloride (0.5 g, 2.7 mmol), pyrazole (0.71 g, 10.36 mmol), N,*N*-diisopropylethylamine (3.55 mL, 20.63 mmol), and dry THF was added to a two-neck, round bottom flask equipped with a condenser. The reaction mixture was heated at 80 °C under N_2 for 23 h. After cooling to room temperature, the solvent was removed under vacuum. The crude product was then washed with DI water. The white solid was collected on a funnel by suction filtration, washed by DI water (3 × 15 mL), and then further purified by a silica gel column (with CH_2Cl_2/methanol 12:1 as the eluent) to provide a white solid (745 mg, 98%). ^{1}H NMR (600 MHz, $CDCl_3$): δ (ppm) = 8.82 (s, 3 H; Pz*H*), 7.98 (s, 3 H; Pz*H*), 6.62 (s, 3 H; Pz*H*). ^{13}C NMR (150 MHz, $CDCl_3$): δ (ppm) = 163.70, 146.13, 130.77, 110.48.

3. Results and discussion

3.1. Synthesis and characterization

The synthesis procedure of P1 and P2 is shown in Scheme 1. Firstly, 1-trityl-1*H*-pyrazol-4-ylboronate pinacol ester (1) was prepared according to reported procedure [44]. Subsequent suzuki coupling of 1 with 4,7-dibromobenzothiadiazole using 1 mol % $Pd(PPh_3)_4$ in 1,2-dimethoxyethane (DME) afford the trityl-protected 2 in a yield of 81%. Removal of the trityl group is achieved using TFA to get the D-A type monomer M1 as a yellow solid in a yield of 84%. The desired conjugated microporous polymer P1 was synthesized in a yield of 80% as an orange solid by refluxing a mixture of cyanuric chloride and M1 in the presence of N,N'-diisopropylethylamine (DIPEA) in THF. In contrast to two reaction monomers (M1 and cyanuric chloride), P1 is insoluble in organic solvents which can be purified easily by repeated washing with organic solvents (e.g. THF). P2 was prepared similarly to P1 with a modest yield of 65%. In order to confirm the bond formation in the synthesis of polymers, a model compound 4 (Scheme 2) was successfully synthesized by reacting cyanuric chloride with excess pyrazole using the same condition in a quantitative yield.

Completion of the reaction was confirmed by the energy-dispersive X-ray spectroscopy (EDX) experiment. As shown in Figs. S1 and S2, P1 is comprised of C, N and S three major elements, while P2 contains C and N two major elements. These results are consistent with the formation of the porous polymer framework. No obvious Cl signal was observed, confirming the completion of the reaction. It is worthy to note that no signal of Pd was observed, indicating no Pd metal residue in P1 and P2. Furthermore, inductively coupled plasma optical emission spectrometry (ICP-OES) test was conducted for monomers M1 and M2, clearly showing no Pd content. Since the polymerization reaction is a metal-free catalytic reaction, we can conclude that there is no Pd residue in polymers.

Figs. 1 and S3 show the XPS spectra of P1 and P2. The results of X-ray photoelectron spectroscopy (XPS) are consistent with the element type and valence state of the porous polymers. As shown in Fig. 1, in addition to H element, the mainly elements involve C, N, S, the peaks located at 284.6 eV are assigned to C-C/C = C, the peaks of 287.7 eV belong to the C = N, the peaks of 290.4 eV are originated from the C–N, the peaks located at 398.8 eV belong to the nitrogen atom of triazine ring, the peaks of 400.5 eV are assigned to the nitrogen atom of benzothiadiazole and pyrazole moieties.

The solid-state ^{13}C NMR experiment was performed to verify the polymer structure. All carbon environments have been identified, confirming the structure of the obtained polymers. Fig. 2a shows the solid-state ^{13}C NMR spectrum of P1. The aromatic region of the solid-state ^{13}C NMR spectrum of P1 is dominated by four distinct peaks (160.4, 150.1, 142.2, and 120.3 ppm). The three downfield signals at 160.4, 150.1 and 142.2 ppm can be assigned to the aromatic carbon atoms adjacent to N atom in the triazine, benzothiadiazole and pyrazole rings, respectively. All other carbon signals were fused into a big broad upfield signal at 120.3 ppm. In addition, the ^{13}C NMR of monomer M1 and model compound 4 (Fig. 2b and c) have also been recorded and analyzed, which match that of P1 pretty well, further verifying the efficiency of the polymerization reaction. Furthermore, the results of elemental analysis (e.g., of C, H, and N) are consistent with the formation of these two polymer frameworks. Thermogravimetric analysis (TGA, Figs. S4 and S5) of the as-prepared porous polymers under N_2 unveils modest-to-high thermal stability. The decomposition temperatures (defined as the temperatures of 5% mass loss) for P1 and P2 were determined to be 160 and 200 °C, respectively.

To gain insight into the structural details and morphology of the polymer, powder X-ray diffraction (PXRD), scanning electron microscopy (SEM), transmission electron microscopy (TEM) analyses and gas sorption were performed. Powder X-ray diffraction (PXRD) measurement of the polymer showed three very broad peaks, suggesting a rather low degree of crystallinity of the polymer solid (Fig. S6). The morphologies of the solid state of P1 and P2 were investigated by scanning electron microscopy (SEM). As shown in Figs. 3a and S7a, as-synthesized polymers show globular aggregates with dimensions on the submicrometer scale. A closer inspection of the structure of polymers by high-resolution TEM unveils the microporosity structure (Figs. 3b, c and S7b), with the average pore widths determined to be ca. 1 nm. Selected area electron diffraction (SAED) (Fig. S8) indicted no sign of crystallinity of the polymer, consisting with the result of PXRD.

Besides TEM, the porosity of the as-synthesized polymer was also determined by the N_2 adsorption/desorption experiments at 77 K (pressure range: from 38 to 768 mmHg). Brunauer-Emmett-Teller (BET) surface areas were determined to be 128 m^2/g and124 m^2/g for P1 and P2, respectively. BJH desorption pore size distribution analysis method on pore size distribution and pore volume of the N_2 adsorption isotherms (77 K) indicated that both polymers have similar average pore widths of 1.3–1.5 nm and modest pore volumes of 0.15 cm^3/g (Fig. 4), suggesting the presence of significant porosity in the polymer. Compared to the porous polymer reported by Xu and coworkers [42], the average pore widths are larger because of the addition of benzothiadiazole and benzene units.

3.2. Optical and electrochemical properties

The UV–vis diffuse reflectance spectra of polymer P1 and P2 are shown in Fig. 5 and S10. In the solid state, polymer P1 shows broad

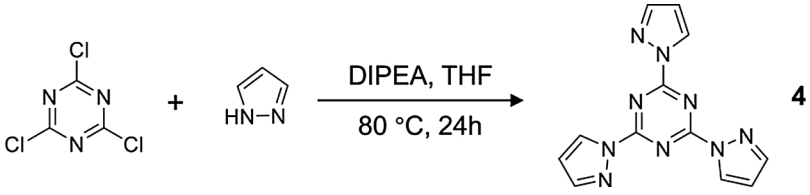

Scheme 2. Synthesis of 4 for model reaction.

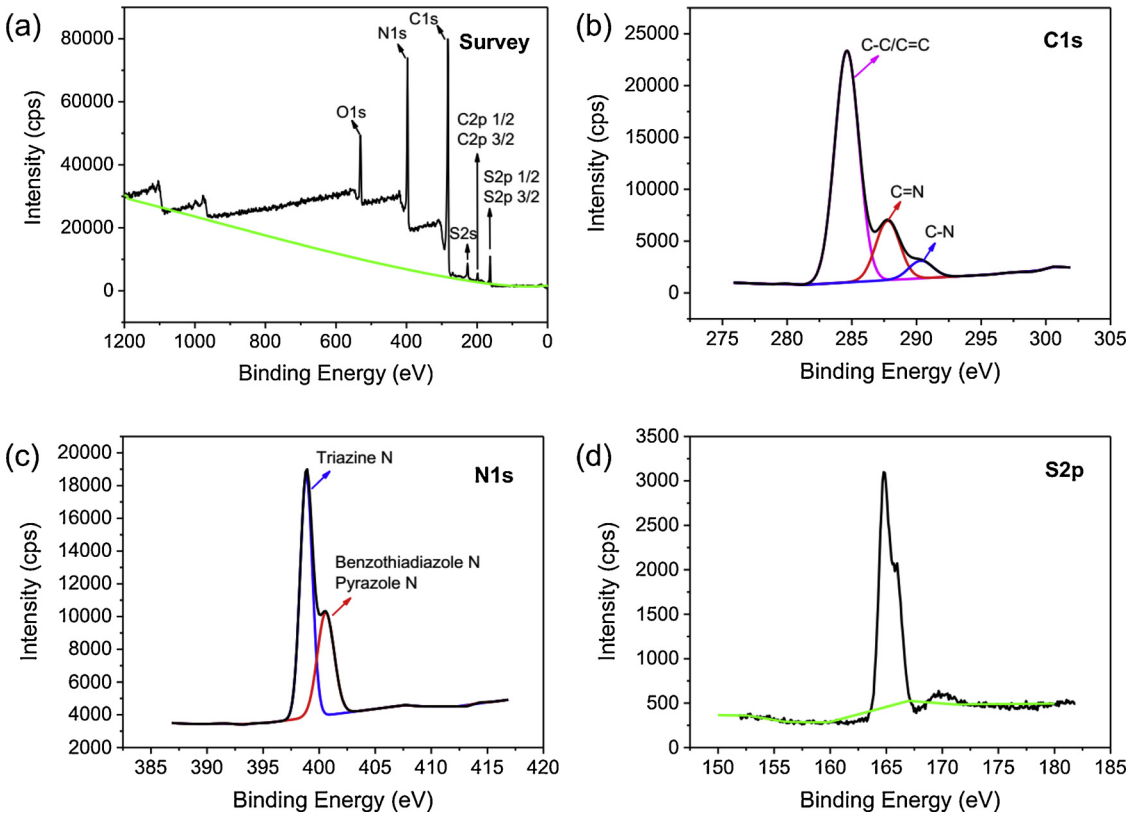

Fig. 1. (a) XPS survey spectrum of P1, and high-resolution XPS spectra of (b) C1s, (c) N1s and (d) S2p for P1.

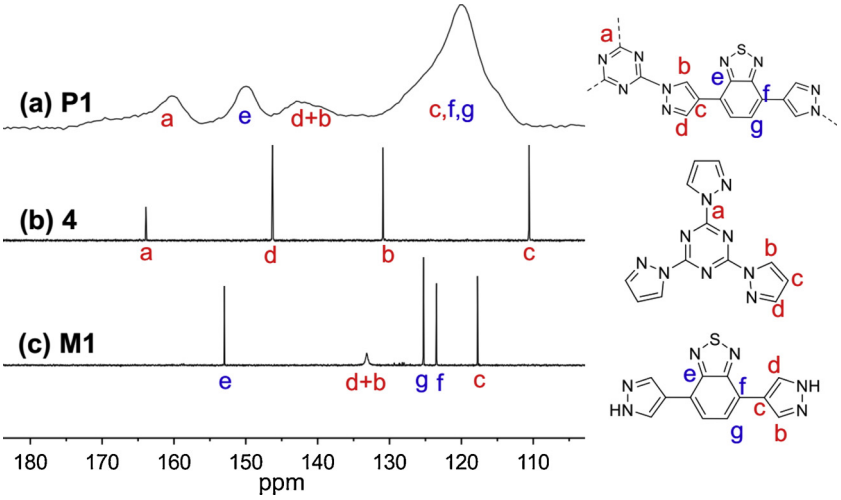

Fig. 2. (a) Solid-state ^{13}C NMR spectrum of P1, and ^{13}C NMR spectra of (b) 4 and (c) M1.

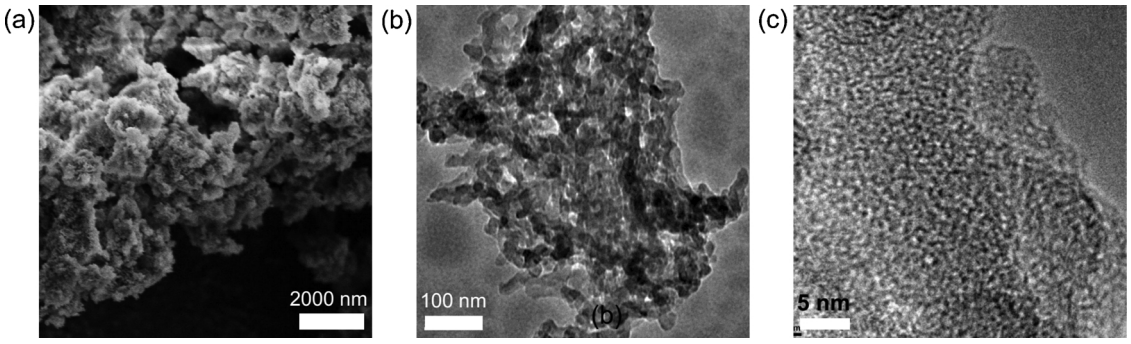

Fig. 3. (a) SEM image, (b) TEM image and (c) HR-TEM image of P1.

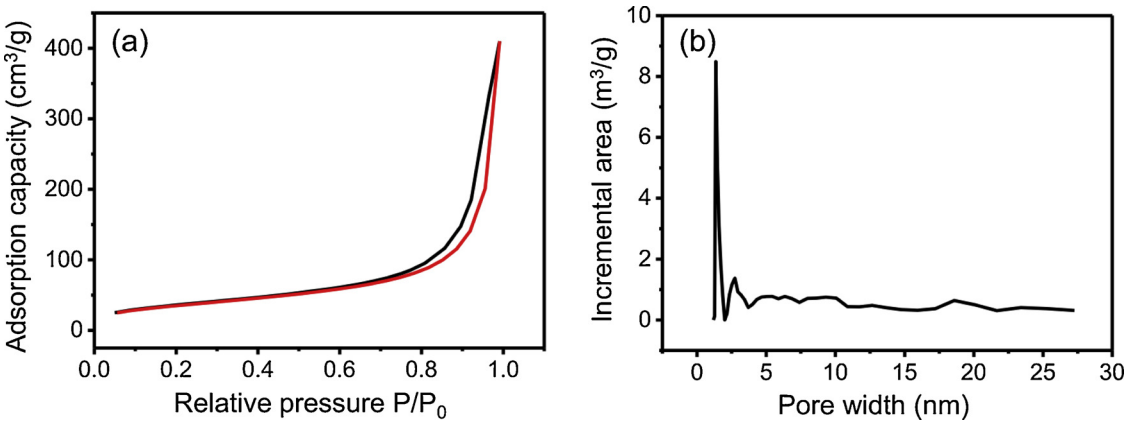

Fig. 4. (a) Nitrogen adsorption isotherm (red line) and desorption isotherm (black line) for P1 recorded at 77 K, (b) profile of the calculated pore size distribution for P1. P/P_0, vapor pressure over saturation pressure. (For interpretation of the references to colour in this figure legend, the reader is referred to the web version of this article).

absorption in the region of 200–500 nm, with the absorption edge extended to approximately 600 nm. The optical bandgap (E_g) calculated from Tauc plots is ca. 2.33 eV for P1 (inset, Fig. 5a), which is ideal for the photocatalytic water splitting considering the light absorbance and reaction over-potentials. By replacing benzene as bridge between two pyrazoles instead of strong electron-accepting benzothiadiazole, P2 exhibits obvious hypochromatic shift in the absorption and larger optical band gap of E_g = 2.94 eV. The maximum emission of P1 and P2 locate at 550 nm and 340 nm, with the fluorescence lifetimes of 0.98 ns and 0.76 ns, respectively.

The UV–vis and emission property of monomers M1 and M2 were also investigated, as shown in Fig. S11. In DMF solution, M1 exhibits an intense visible-light absorption with a peak maximum at 435 nm, which is attributed to the pyrazole donor to benzothiadiazole acceptor charge-transfer absorption. In contrast, M2 shows a relatively weak visible light absorption with a peak maximum at 285 nm, due to the lack of strong charge transfer. The UV–vis absorption of polymers in the solid state show obvious red shift compared to their monomers due to the partial stacking of conjugated backbone. However, dispersion of the polymers in solution shows similar absorption and emission spectra compared to their monomers. The reason is due to that the triazine unit is linked to the nodes at pyrazoles of M1 and M2, limiting the effective conjugation length. This is consistent with the theoretical calculation (vide infra).

Cyclic voltammogram (CV) measurement was carried out to further investigate the electrochemical properties of the P1 and P2. As shown in Figs. 5b and S10, both polymers show one reversible reduction. From the onset of the reductive peak in CV, the LUMO levels of P1 and P2 were determined to be -0.42 eV and -0.44 eV (v.s. SHE). The HOMO levels were calculated to be 1.91 eV and 2.50 eV (v.s. SHE) based on the equation of $E_g = E_{LUMO}\text{-}E_{HOMO}$.

DFT calculations of the fragmental structures of P1 were carried out to gain insightful information of its electronic properties. As shown in Fig. 5d, the electron density of the HOMO is considerably delocalized over the extended conjugated pyrazole-benzothiadiazole-pyrazole moiety. The LUMO mainly reside on the π* orbital of the

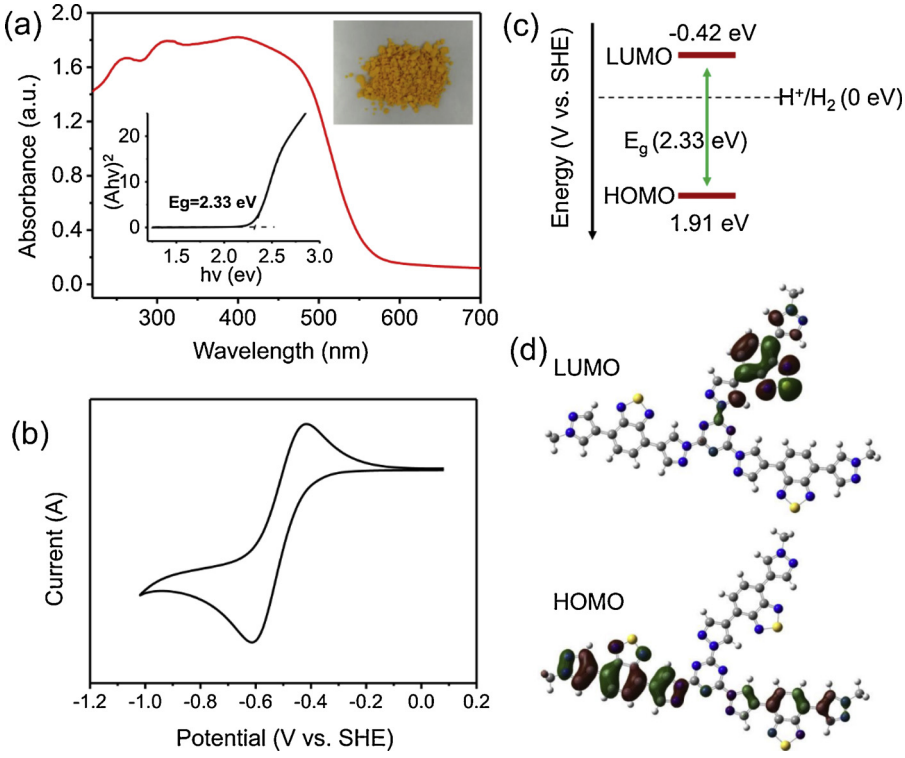

Fig. 5. (a) UV–vis diffuse reflectance spectra of P1. The inset shows optical image of P1 and the Tauc plots. The intersection of two dashed lines indicates the value of estimated optical bandgap. (b) Cyclic voltammogram (CV) curve of P1. Scan rate = 50 mV/s. (c) Calculated HOMO and LUMO band position of P1. (d) DFT calculated frontier molecular orbitals for truncated P1.

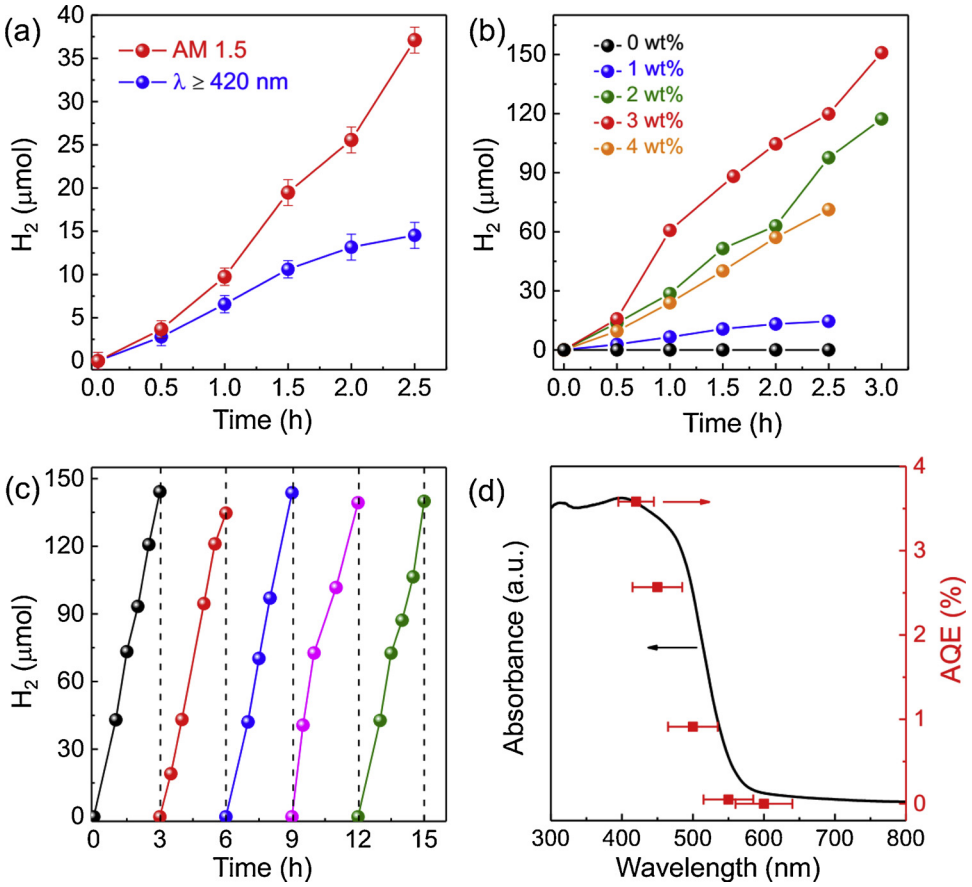

Fig. 6. (a) Temporal photocatalytic H_2 production using P1 under simulated sun light (AM 1.5) and visible-light illumination (λ ≥ 420 nm) in the presence of TEOA, 1 wt% Pt was loaded as a co-catalyst. (b) Temporal H_2 production for P1 loaded with different amounts of Pt co-catalyst under visible light (λ ≥ 420 nm). (c) Stability tests using photocatalyst P1 under visible light (λ ≥ 420 nm) for 15 h (3 wt% Pt as co-catalyst). (d) Action spectrum (apparent quantum efficiency (AQE) vs. excitation wavelength) of photocatalyst P1, 3 wt% Pt as co-catalyst.

benzothiadiazole unit. However, the contribution of the triazine moiety on the electron density of both HOMO and LUMO is small, because of the poor electronic communication resulting from the nodes at pyrazole nitrogen atom. Overall, the theoretical calculations fully support the photophysical properties of these novel materials.

3.3. Photocatalytic hydrogen evolution

We then investigated the activity of P1 and P2 for photocatalytic water reduction reactions, both under simulated sun light (AM 1.5) and visible light illumination (λ ≥ 420 nm). The results are illustrated in Figs. 6 and S12. All the photocatalytic tests of sample were carried out in the presence of sacrificial agent (water: triethanolamine = 9:1, v/v), where triethanolamine (TEOA) acts as a hole scavenger to promote photo-reduction reactions. Pt from H_2PtCl_6 thermo-decomposition served as the co-catalyst for H_2 evolution. Control experiments without either light or photocatalyst give no hydrogen evolution, precluding any spontaneous reactions that may lead to hydrogen production. As shown in Fig. 6, continuous hydrogen evolution has been realized on polymer P1 under current testing conditions (TEOA, 1 wt% Pt) both under simulated sun light (AM 1.5) and visible light illumination (λ ≥ 420 nm), indicating real photocatalytic processes. In particular, the sample maintained almost half of the activity using visible light photons to that under AM 1.5, confirming visible-light-active photocatalyst (Fig. 6a). Besides, its activity shows a strong dependence on the amounts of Pt loaded, with negligible activity in absence of Pt and maximal HER of 50 μmol h^{-1} at 3 wt% loading point (Fig. 6b). Considering the small amounts of sample powders used in the experiments (50 mg), more than 150 μmol hydrogen was produced within 3 h under visible light illumination, highlighting the efficacy of this new compound for photocatalytic hydrogen production. The reaction stability of the polymer P1 was further examined by repeated cycles of light illumination for hydrogen production (Fig. 6c). The reactivity of polymer P1 was maintained for five cycles of experiment, suggesting good stability. Its light-dependent activity was also confirmed by action spectra where monochromic light was used as a photon source. Its activity shows a good match with its UV–vis absorption spectrum, indicating real photon-driven catalytic processes. Its apparent quantum efficiency approaches as high as 3.6% (Fig. 6d), surpassing or at least comparable to the state-of-art conjugated organic photocatalysts.

As a control experiment, the HER of P2 was also investigated in order to study the D-A structure on the photocatalytic property. Under the same photocatalytic condition (TEOA, 1 wt% Pt), P2 shows very low hydrogen evolution rates with under both visible light (0.2 μmol h^{-1}, λ ≥ 420 nm) and AM1.5 (0.9 μmol h^{-1}, AM 1.5), compared to P1 (5.6 μmol h^{-1}, λ ≥ 420 nm; 14.8 μmol h^{-1}, AM 1.5). Similarly, its visible-light activity shows a strong dependence on the amounts of Pt loaded, with maximal HER of 0.9 μmol h^{-1} at 3 wt% Pt loading point, which is still much lower than that of P1 (50 μmol h^{-1}). The above results highlight the pivotal role of the D-A structure in P1 for better photocatalytic performance due to its broad and visible light absorption. In addition, the longer fluorescence lifetime of P1 would enhance the transfer of the electron at LUMO level to the Pt co-catalyst that subsequently reduced water to hydrogen. As another control experiment, monomer M1 did not shows any photocatalyst activities using TEOA as sacrificial donor and a Pt co-catalyst, indicating the important role of both the porosity and triazine unit. We also studied oxygen evolution to probe whether full water splitting is possible with the P1 and P2. However, no O_2 could be detected under the conditions used. Overall, multiple factors such as porosity, wider range of visible light absorption and longer fluorescence lifetime all contribute to the high performance of P1.

4. Conclusion

In summary, a simple, efficient and metal-free catalytic synthesis method was used to synthesize two triazine-based conjugated porous polymers P1 and P2 for visible-light driven hydrogen generation. The identity, porosity and optical property of these two materials were fully characterized by multiple techniques. Comparable to many other CMP, these materials have low degree of crystalline order in the solid state, with BET surface area of 124-128 m^2/g and average pore width of ca. 1 nm. Notably, P1 has the ideal optical band gap of about 2.3 eV, and exhibits a high efficiency for photocatalytic H_2 evolution under visible light ($\lambda \geq 420$ nm), due to the introduction of D-A structure in the backbone. In contrast, P2 with similar porosity but less visible-light absorbance exhibits poor hydrogen evolution property. Our results reveal the important roles of porosity, wider range of visible light absorption and excited state lifetime on the high performance of photocatalytic hydrogen evolution of P1. We believe that this simple approach to link D-A type light-absorbing unit by triazine unit through simple reaction of cyanuric chloride and pyrazole will generate a large family of band-gap tunable CMPs for efficient water splitting. Future studies will involve the expansion of this class of conjugated porous polymer with different D-A units for photocatalytic water splitting, and will be reported in due course.

Conflict of interest

There are no conflicts to declare.

Acknowledgements

This work was supported by the National Natural Science Foundation of China (51703166, 21401142) and Natural Science Foundation of Shanghai (19ZR1459200). X.H. and X. X. thanks the National 1000-Plan Program for support. We thank Prof. Yi Ren at ShanghaiTech University for his kind help with the DFT calculation.

Appendix A. Supplementary data

Supplementary material related to this article can be found, in the online version, at doi:https://doi.org/10.1016/j.apcatb.2019.117935.

References

[1] G. Zhang, Z.-A. Lan, X. Wang, Conjugated polymers: catalysts for photocatalytic hydrogen evolution, Angew. Chem. Int. Ed. 55 (2016) 15712–15727.
[2] P. Guiglion, C. Butchosa, M.A. Zwijnenburg, Polymer photocatalysts for water splitting: insights from computational modeling, Macromol. Chem. Phys. 217 (2016) 344–353.
[3] A. Kudo, Y. Miseki, Heterogeneous photocatalyst materials for water splitting, Chem. Soc. Rev. 38 (2009) 253–278.
[4] T. Hisatomi, K. Domen, Progress in the demonstration and understanding of water splitting using particulate photocatalysts, Curr. Opin. Electrochem. 2 (2017) 148–154.
[5] X. Chen, S. Shen, L. Guo, S.S. Mao, Semiconductor-based photocatalytic hydrogen generation, Chem. Rev. 110 (2010) 6503–6570.
[6] K. Maeda, K. Teramura, D. Lu, T. Takata, N. Saito, Y. Inoue, K. Domen, Photocatalyst releasing hydrogen from water, Nature 440 (2006) 295.
[7] X. Chen, L. Liu, P.Y. Yu, S.S. Mao, Increasing solar absorption for photocatalysis with black hydrogenated titanium dioxide nanocrystals, Science 331 (2011) 746–750.
[8] A. Li, X. Chang, Z. Huang, C. Li, Y. Wei, L. Zhang, T. Wang, J. Gong, Thin heterojunctions and spatially separated cocatalysts to simultaneously reduce bulk and surface recombination in photocatalysts, Angew. Chem. Int. Ed. 55 (2016) 13734–13738.
[9] Y. Xiang, X. Wang, X. Zhang, H. Hou, K. Dai, Q. Huang, H. Chen, Enhanced visible light photocatalytic activity of TiO_2 assisted by organic semiconductors: a structure optimization strategy of conjugated polymers, J. Mater. Chem. A 6 (2018) 153–159.
[10] E. Abroshan, S. Farhadi, A. Zabardasti, Novel magnetically separable Ag_3PO_4/$MnFe_2O_4$ nanocomposite and its high photocatalytic degradation performance for organic dyes under solar-light irradiation, Sol. Energy Mater. Sol. Cells 178 (2018) 154–163.
[11] X. Yu, N. Ren, J. Qiu, D. Sun, L. Li, H. Liu, Killing two birds with one stone: to eliminate the toxicity and enhance the photocatalytic property of CdS nanobelts by assembling ultrafine TiO_2 nanowires on them, Sol. Energy Mater. Sol. Cells 183 (2018) 41–47.
[12] S. Yanagida, A. Kabumoto, K. Mizumoto, C. Pac, K. Yoshino, Poly(p-phenylene)-catalysed photoreduction of water to hydrogen, J. Chem. Soc. Chem. Commun. (1985) 474–475.
[13] X. Wang, K. Maeda, A. Thomas, K. Takanabe, G. Xin, J.M. Carlsson, K. Domen, M. Antonietti, A metal-free polymeric photocatalyst for hydrogen production from water under visible light, Nat. Mater. 8 (2008) 76.
[14] G. Liu, T. Wang, H. Zhang, X. Meng, D. Hao, K. Chang, P. Li, T. Kako, J. Ye, Nature-inspired environmental "phosphorylation" boosts photocatalytic H_2 production over carbon nitride nanosheets under visible-light irradiation, Angew. Chem. Int. Ed. 54 (2015) 13561–13565.
[15] J. Liu, Y. Liu, N. Liu, Y. Han, X. Zhang, H. Huang, Y. Lifshitz, S.-T. Lee, J. Zhong, Z. Kang, Metal-free efficient photocatalyst for stable visible water splitting via a two-electron pathway, Science 347 (2015) 970–974.
[16] D.J. Woods, R.S. Sprick, C.L. Smith, A.J. Cowan, A.I. Cooper, A solution-processable polymer photocatalyst for hydrogen evolution from water, Adv. Energy Mater. 7 (2017) 1700479.
[17] L. Li, R.G. Hadt, S. Yao, W.-Y. Lo, Z. Cai, Q. Wu, B. Pandit, L.X. Chen, L. Yu, Photocatalysts based on cobalt-chelating conjugated polymers for hydrogen evolution from water, Chem. Mater. 28 (2016) 5394–5399.
[18] R.S. Sprick, L. Wilbraham, Y. Bai, P. Guiglion, A. Monti, R. Clowes, A.I. Cooper, M.A. Zwijnenburg, Nitrogen containing linear poly(phenylene) derivatives for photo-catalytic hydrogen evolution from water, Chem. Mater. 30 (2018) 5733–5742.
[19] R.S. Sprick, Catherine M. Aitchison, E. Berardo, L. Turcani, L. Wilbraham, B.M. Alston, K.E. Jelfs, M.A. Zwijnenburg, A.I. Cooper, Maximising the hydrogen evolution activity in organic photocatalysts by co-polymerisation, J. Mater. Chem. A 6 (2018) 11994–12003.
[20] R.S. Sprick, B. Bonillo, R. Clowes, P. Guiglion, N.J. Brownbill, B.J. Slater, F. Blanc, M.A. Zwijnenburg, D.J. Adams, A.I. Cooper, Visible-light-driven hydrogen evolution using planarized conjugated polymer photocatalysts, Angew. Chem. Int. Ed. 55 (2016) 1792–1796.
[21] C. Yang, B.C. Ma, L. Zhang, S. Lin, S. Ghasimi, K. Landfester, K.A.I. Zhang, X. Wang, Molecular engineering of conjugated polybenzothiadiazoles for enhanced hydrogen production by photosynthesis, Angew. Chem. Int. Ed. 55 (2016) 9202–9206.
[22] C. Cheng, X. Wang, Y. Lin, L. He, J.-X. Jiang, Y. Xu, F. Wang, The effect of molecular structure and fluorination on the properties of pyrene-benzothiadiazole-based conjugated polymers for visible-light-driven hydrogen evolution, Polym. Chem. 9 (2018) 4468–4475.
[23] L. Li, Z. Cai, Q. Wu, W.-Y. Lo, N. Zhang, L.X. Chen, L. Yu, Rational design of porous conjugated polymers and roles of residual palladium for photocatalytic hydrogen production, J. Am. Chem. Soc. 138 (2016) 7681–7686.
[24] R.S. Sprick, B. Bonillo, M. Sachs, R. Clowes, J.R. Durrant, D.J. Adams, A.I. Cooper, Extended conjugated microporous polymers for photocatalytic hydrogen evolution from water, Chem. Commun. 52 (2016) 10008–10011.
[25] L. Li, W.-y. Lo, Z. Cai, N. Zhang, L. Yu, Donor–acceptor porous conjugated polymers for photocatalytic hydrogen production: the importance of acceptor comonomer, Macromolecules 49 (2016) 6903–6909.
[26] L. Li, Z. Cai, Structure control and photocatalytic performance of porous conjugated polymers based on perylene diimide, Polym. Chem. 7 (2016) 4937–4943.
[27] L. Wang, Y. Wan, Y. Ding, Y. Niu, Y. Xiong, X. Wu, H. Xu, Photocatalytic oxygen evolution from low-bandgap conjugated microporous polymer nanosheets: a combined first-principles calculation and experimental study, Nanoscale 9 (2017) 4090–4096.
[28] X. Wang, L. Chen, S.Y. Chong, M.A. Little, Y. Wu, W.-H. Zhu, R. Clowes, Y. Yan, M.A. Zwijnenburg, R.S. Sprick, A.I. Cooper, Sulfone-containing covalent organic frameworks for photocatalytic hydrogen evolution from water, Nat. Chem. 10 (2018) 1180–1189.
[29] P. Pachfule, A. Acharjya, J. Roeser, T. Langenhahn, M. Schwarze, R. Schomäcker, A. Thomas, J. Schmidt, Diacetylene functionalized covalent organic framework (COF) for photocatalytic hydrogen generation, J. Am. Chem. Soc. 140 (2018) 1423–1427.
[30] M.G. Schwab, M. Hamburger, X. Feng, J. Shu, H.W. Spiess, X. Wang, M. Antonietti, K. Müllen, Photocatalytic hydrogen evolution through fully conjugated poly(azomethine) networks, Chem. Commun. 46 (2010) 8932–8934.
[31] L. Wang, R. Fernández-Terán, L. Zhang, D.L.A. Fernandes, L. Tian, H. Chen, H. Tian, Organic polymer dots as photocatalysts for visible light-driven hydrogen generation, Angew. Chem. Int. Ed. 55 (2016) 12306–12310.
[32] P.B. Pati, G. Damas, L. Tian, D.L.A. Fernandes, L. Zhang, I.B. Pehlivan, T. Edvinsson, C.M. Araujo, H. Tian, An experimental and theoretical study of an efficient polymer nano-photocatalyst for hydrogen evolution, Energy Environ. Sci. 10 (2017) 1372–1376.
[33] K. Wang, L.-M. Yang, X. Wang, L. Guo, G. Cheng, C. Zhang, S. Jin, B. Tan, A. Cooper, Covalent triazine frameworks via a low-temperature polycondensation approach, Angew. Chem. Int. Ed. 56 (2017) 14149–14153.
[34] C.B. Meier, R.S. Sprick, A. Monti, P. Guiglion, J.-S.M. Lee, M.A. Zwijnenburg, A.I. Cooper, Structure-property relationships for covalent triazine-based frameworks: the effect of spacer length on photocatalytic hydrogen evolution from water, Polymer 126 (2017) 283–290.
[35] J. Bi, W. Fang, L. Li, J. Wang, S. Liang, Y. He, M. Liu, L. Wu, Covalent triazine-based frameworks as visible light photocatalysts for the splitting of water, Macromol. Rapid Commun. 36 (2015) 1799–1805.
[36] K. Schwinghammer, S. Hug, M.B. Mesch, J. Senker, B.V. Lotsch, Phenyl-triazine oligomers for light-driven hydrogen evolution, Energy Environ. Sci. 8 (2015)

3345–3353.
[37] S. Kuecken, A. Acharjya, L. Zhi, M. Schwarze, R. Schomäcker, A. Thomas, Fast tuning of covalent triazine frameworks for photocatalytic hydrogen evolution, Chem. Commun. 53 (2017) 5854–5857.
[38] L. Stegbauer, K. Schwinghammer, B.V. Lotsch, A hydrazone-based covalent organic framework for photocatalytic hydrogen production, Chem. Sci. 5 (2014) 2789–2793.
[39] V.S. Vyas, F. Haase, L. Stegbauer, G. Savasci, F. Podjaski, C. Ochsenfeld, B.V. Lotsch, A tunable azine covalent organic framework platform for visible light-induced hydrogen generation, Nat. Commun. 6 (2015) 8508.
[40] F. Haase, T. Banerjee, G. Savasci, C. Ochsenfeld, B.V. Lotsch, Structure–property–activity relationships in a pyridine containing azine-linked covalent organic framework for photocatalytic hydrogen evolution, Faraday Discuss. 201 (2017) 247–264.
[41] Y. Xu, S. Jin, H. Xu, A. Nagai, D. Jiang, Conjugated microporous polymers: design, synthesis and application, Chem. Soc. Rev. 42 (2013) 8012–8031.
[42] J. Liu, K.-K. Yee, K.K.-W. Lo, K.Y. Zhang, W.-P. To, C.-M. Che, Z. Xu, Selective Ag(I) binding, H_2S sensing, and white-light emission from an easy-to-make porous conjugated polymer, J. Am. Chem. Soc. 136 (2014) 2818–2824.
[43] H.J. Son, F. He, B. Carsten, L. Yu, Are we there yet? Design of better conjugated polymers for polymer solar cells, J. Mater. Chem. A 21 (2011) 18934–18945.
[44] L.J. Kershaw Cook, R. Kearsey, J.V. Lamb, E.J. Pace, J.A. Gould, Efficient and chromatography-free methodology for the modular synthesis of oligo-(1H-pyrazol-4-yl)-arenes with controllable size, shape and steric bulk, Tetrahedron Lett. 57 (2016) 895–898.
[45] N. Huang, P. Wang, M.A. Addicoat, T. Heine, D. Jiang, Ionic covalent organic frameworks: design of a charged interface aligned on 1D channel walls and its unusual electrostatic functions, Angew. Chem. Int. Ed. 56 (2017) 4982–4986.
[46] F. Yu, Z. Wang, S. Zhang, H. Ye, K. Kong, X. Gong, J. Hua, H. Tian, Molecular engineering of donor–acceptor conjugated polymer/g-C3N4 heterostructures for significantly enhanced hydrogen evolution under visible-light irradiation, Adv. Funct. Mater. 28 (2018) 1804512.
[47] Y. Xiang, X. Wang, L. Rao, P. Wang, D. Huang, X. Ding, X. Zhang, S. Wang, H. Chen, Y. Zhu, Conjugated polymers with sequential fluorination for enhanced photocatalytic H_2 evolution via proton-coupled electron transfer, ACS Energy Lett. 3 (2018) 2544–2549.
[48] J. Chen, C.-L. Dong, D. Zhao, Y.-C. Huang, X. Wang, L. Samad, L. Dang, M. Shearer, S. Shen, L. Guo, Molecular design of polymer heterojunctions for efficient solar–hydrogen conversion, Adv. Mater. 29 (2017) 1606198.